# Dynamic response and energy loss in jointed structures using finite element methods: application to an aero-engine casing assembly

**X. Chi[1], D. Di Maio[2], N. A. J. Lieven[1]**
[1] Department of Aerospace Engineering, University of Bristol, Queens Building, University Walk, Bristol, BS8 1TR, England, UK

[2] Department of Mechanical Engineering, University of Bristol, Queens Building, University Walk, Bristol, BS8 1TR, England, UK
e-mail: **xintian.chi@bristol.ac.uk**

## Abstract
The purpose of this research is to identify the influences caused by local changes in contact regions of an aero-engine casing assembly on its dynamic and thermal behaviours through Finite Element (FE) methods. The creation and updates of the FE model are demonstrated in this paper. Two types of FE analyses are performed in this research. The first analysis is in the frequency domain, which focuses on the changes in natural frequencies caused by the different contact conditions. The second analysis is in the time domain to study the changes in frictional heat generation caused by alternate contact conditions of the interface regions.

In the concluding observations of this paper, results from these two types of analyses are interpreted to demonstrate that the local changes in contact regions can alter the dynamic and thermal responses of the aero-engine casing assembly by affecting several determining parameters differentially, and these changes caused by the different contact conditions are summarised, analysed and explained.

## 1 Introduction

Engineering structures are tending to become more complex with an increasing number of components. The components are usually connected by bolts, which creates jointed interfaces. There is a possibility that these joints and interfaces can cause noticeable changes to the dynamic and thermal behaviours of the structure, which must be fully understood to ensure the structure functions stably and safely.

There are several parameters that may determine the effects caused by the joints and the interfaces, which include the bolt preload, material type and size of the bolts, contact area of the interface regions, and bolt tightening sequence [1]. This research focuses on the influences caused specifically by changes in the contact area of the interface regions.

Experimental studies on the effects caused by different contact areas can be arduous because it requires several samples of the structure to be made, each having a contact region with a different profile. These experimental tests are economically achievable for small and simple structures that do not require high manufacturing time and cost. However, due to the fact that the dynamic behaviours of larger and more complex structures are more difficult to predict, analyses of these structures appear to be more necessary.

The structure being studied in this research is an aero-engine casing assembly, which has three components: a Combustion Chamber Outer Casing (CCOC), a High-Pressure Chamber (HPC) and a Low-Pressure Chamber (LPC). There are two jointed interfaces in this assembly, which are between the CCOC and HPC and between the HPC and LPC. As explained above, making several samples of this complex structure for experimental testing is economically impractical. Instead, Finite Element (FE) methods can be used.

In the preparation phase of this research, the dimensions of the aero-engine casing assembly are measured, based on which a preliminary FE model is created. The FE model is then updated according to the modal parameters acquired from an Experimental Modal Analysis (EMA). Two criteria, the Modal Assurance Criterion (MAC) and Natural Frequency Difference (NFD), are used to evaluate the updated FE model. After the FE model is updated to an acceptable level, subsequent FE models are created, which all have contact interfaces with different profiles.

Firstly, a frequency domain FE modal analysis is performed on each model. The natural frequency is selected as the parameter to be studied, which aims to identify the effects caused by the different profiles of the contact regions on the dynamic responses and modal parameters of the structure. Strain energy density is used to analyse and explain the changes in the natural frequencies.

After the completion of the frequency domain analysis, several simplified models are created for the time domain coupled temperature-displacement dynamic analysis. In the time domain analysis, each model is excited by a single-point sinusoidal force for a same amount of time. The thermal data, namely temperature increase and frictional heat generation, at the end of each analysis are collected to evaluate the changes in friction and energy loss caused by the different contact conditions of the interface regions.

## 2 Preliminary FE modelling and frequency domain modal analysis

In the first stage of this research, an FE model of the aero-engine casing assembly needs to be created. The structure is composed of three parts – a CCOC, an HPC and an LPC, as shown in Figure 1 (a). The CCOC and HPC are connected by 60 bolts and the HPC and LPC are connected by 80 bolts. The total mass of the aero-engine casing assembly is 266 kg, with the exact dimensions and material properties being unknown.

The dimensions of the aero-engine casing assembly are measured, based on which a preliminary FE model is created. Most major geometric features are included in the FE model. Minor features that are considered unable to alter its dynamic behaviours significantly are excluded from the FE model to reduce computational time. The created preliminary FE model is shown in Figure 1 (b).

It is not necessary to model the bolts physically because the FE software Abaqus has built-in engineering fastener features that can be used to simulate the bolts while saving the computational costs. 140 engineering fasteners are added corresponding to their actual locations, for which proper connector properties are defined so that stiffness properties are added for one Degree of Freedom (DOF), with the other DOFs being fully constrained [2]. The interaction properties are defined for the interface regions so that there are tangential behaviours which model the friction, normal behaviours which prevent penetration of the surfaces [3], as well as thermal behaviours including heat generation and thermal conductance which model the heat generation and transfer that will be involved in the time domain analysis section of this research.

As for material properties, because the exact material of the structure is unknown, a density value of $4.25 \times 10^3$ kg/m$^3$ is used, so the total mass of the FE model matches the real mass of the structure. A Young's modulus value of 100 GPa is used in this preliminary model for the ease of model update as it is between the Young's modulus of several potential materials of this structure. Similarly, a Poisson's ratio value of 0.30 is used. The boundary condition is set to be free-free to match the condition in the EMA.

(a) (b)

Figure 1: The aero-engine casing assembly and its FE model

The FE analysis step used in this part is a frequency domain eigenvalue extraction procedure that calculates the natural frequencies and mode shapes of the structure. The first 20 no-rigid modes are requested to match the number of modes from EMA. Lanczos algorithm is used because of its general capabilities [4].

The last step before the FE simulation becoming executable is to mesh the structure. Considering that during this step of the analysis, the parameters being studied are the natural frequencies and mode shapes of the structure and that 20 modes are studied, it is essential to create a fine-mesh model of the entire structure. A coarse mesh on any part of the structure is possible to cause inaccuracies in the results of at least one mode.

Due to the high complexity of the structure, only the tetrahedral element shape is usable. Mesh convergence is performed to calculate the proper element size, which decides that a 20 mm global element size with 10% minimum element size control is small enough to obtain accurate results. However, because the profiles of the interfaces will be changed which creates smaller areas, the element size of these regions is further decreased to 5 mm for improved accuracy. Eventually, the interface regions have a 5 mm initial element size and 0.5 mm minimum element size. The rest of the model has a 20 mm initial element size and 2 mm minimum element size. The results from the FE modal analysis will be shown in the next section.

## 3 Experimental Modal Analysis (EMA) results and model updates

An EMA is performed on this aero-engine casing assembly to measure the natural frequencies and mode shapes of the first 20 non-rigid modes of the structure. The results of natural frequencies from the EMA are shown in Table 1. The first 10 mode shapes from the EMA are shown in Figure 2. Because of the symmetry of the structure, each mode has its pair with almost identical natural frequency and mode shape. Only the first 10 modes are used for the model updates, as keeping the accuracy of FEA results will be increasingly difficult for higher order modes because of more complex deformation shapes and dynamic responses.

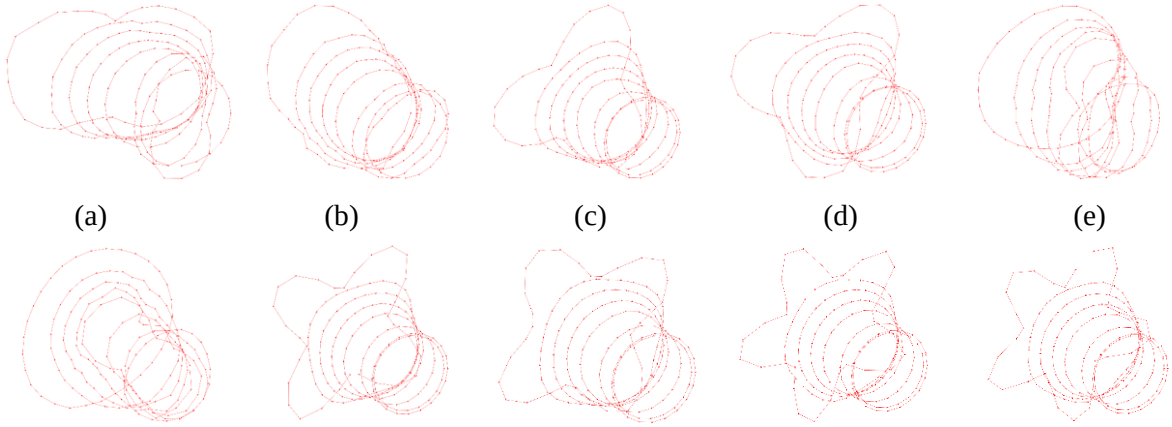


Figure 2: Mode shapes of the first 10 non-rigid modes measured from EMA

The results of the natural frequencies calculated from the FE analysis and their differences from the EMA results are listed in Table 2. The NFD is used to compare the natural frequencies from EMA and FE modal analysis, which is defined as shown in Equation 1, where $f_{FE}$ is the natural frequency calculated from FE modal analysis, and $f_{EMA}$ is the natural frequency calculated from EMA.

$$\text{NFD} = \frac{f_{FE} - f_{EMA}}{f_{EMA}} \times 100\% \tag{1}$$

The mode shapes calculated from the FE modal analysis are shown in Figure 3.

| Mode | 1 | 2 | 3 | 4 | 5 | 6 | 7 | 8 | 9 | 10 |
|---|---|---|---|---|---|---|---|---|---|---|
| Freq (Hz) | 39.141 | 39.685 | 53.128 | 53.21 | 58.51 | 58.935 | 82.256 | 82.348 | 125.73 | 125.8 |
| Mode | 11 | 12 | 13 | 14 | 15 | 16 | 17 | 18 | 19 | 20 |
| Freq (Hz) | 180.50 | 180.56 | 187.68 | 189.35 | 196.75 | 201.06 | 206.03 | 229.84 | 230.28 | 232.72 |

Table 1: Natural frequencies of the first 20 non-rigid modes measured from EMA

| Mode | 1 | 2 | 3 | 4 | 5 | 6 | 7 | 8 | 9 | 10 |
|---|---|---|---|---|---|---|---|---|---|---|
| Freq (Hz) | 38.951 | 39.129 | 60.304 | 60.307 | 75.056 | 75.119 | 99.926 | 99.932 | 155.51 | 155.52 |
| NFD (%) | -0.49 | -1.40 | 13.51 | 13.34 | 28.28 | 27.46 | 21.48 | 21.35 | 23.69 | 23.62 |

Table 2: Natural frequencies of the first 10 non-rigid modes calculated from the preliminary FE analysis

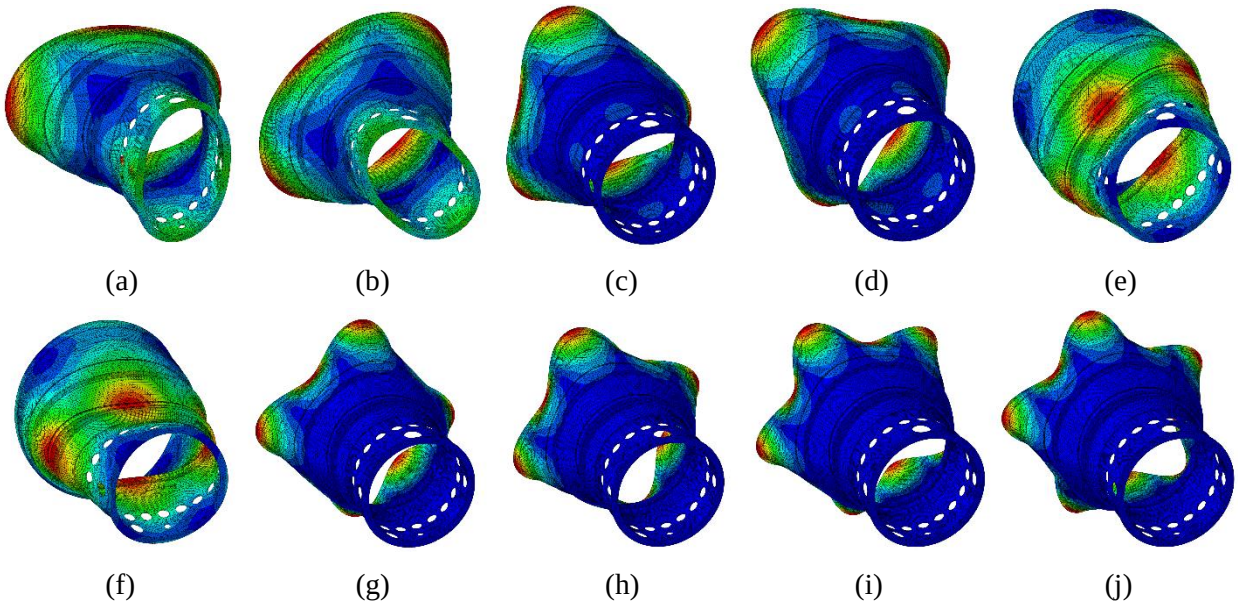


Figure 3: Mode shapes of the first 10 non-rigid modes calculated from the preliminary FE analysis

It can be observed that, although there are discrepancies between natural frequencies, in general the mode shapes and their sequences in the FE modal analysis results match those in the EMA results. However, it is important to note that, despite the visual agreements in the mode shapes between the FE results and EMA results, quantitative methods are still required to evaluate the correlations.

Before comparing the mode shapes quantitatively, the first step of model update should be improving NFD. Theoretically, the entire model updating process can be completed automatically as there are several software packages available to perform this task, most of which update the model based on NFD and MAC. However, these engineering fasteners used in this model, as explained in the previous section, are part of the built-in features of Abaqus, hence unable to be read and processed by the model updating software.

There are several potential solutions to this problem. Firstly, the bolts can be modelled without using the engineering fastener features so that they can be processed by the model updating software. However, modelling the bolts will increase the number of components in this structure. Moreover, these bolts will require high-quality mesh with very small element sizes, which increases computational cost significantly.

The second solution is to update the three components separately using modal updating software. This method requires the mass properties and modal parameters of each component of the structure, which needs disassembly of the structure. Considering the difficulties in practical execution, this solution is not optimal.

The third solution involves editing the input file generated by Abaqus that is going to be imported into model updating software, where the sections containing the engineering fasteners can be forced to be skipped by

the model updating software and added back when the model updating software uses Abaqus as the external solver to perform FE modal analyses with the updated parameters. However, this method is only achievable if the model updating software interacts with Abaqus and uses Abaqus as the external solver.

The last solution, which is most general and straightforward, is to update the model manually without relying on any model updating software. This process seems arduous, but if the relationship between the natural frequencies and the potential determining factors can be found, a manual model update is achievable.

Firstly, the parameters to be updated need to be selected. The determining factors to the modal parameters of the FE model include density, Young's modulus and Poisson's ratio of the material, the geometry of the structure and minor factors such as contact properties and properties of the engineering fasteners.

The geometry of the FE model should be kept unchanged, as changing it will require the largest amount of work. The density of the material for each part is also preferably unchanged because the mass of the FE model already matches the actual mass of the structure. Between Young's modulus and Poisson's ratio, the model update should begin with changing Young's modulus because the Poisson's ratio values of all possible materials are very close, changing Poisson's ratio is not expected to make a considerable difference.

Theoretically, for an undamped system, if the geometry and density remain unchanged, its natural frequencies should be in direct proportion to stiffness. When damping is considered, the positive correlation between natural frequencies and stiffness still exists, although the mathematical relationship becomes more complicated. Changing Young's modulus of material will alter the stiffness matrix of the structure. A higher value of Young's modulus will increase the natural frequencies of the structure because of the increased stiffness. Following this relationship between Young's modulus and natural frequency, it is possible to perform the model update iteratively in a more strategic way.

By inspecting the results in Table 2, it can be observed that apart from the first two modes, all other FE modes appear to have higher natural frequencies, which indicates the overall stiffness of the FE model is higher than the actual value. Reducing the Young's modulus of all three components blindly can be misleading, as the natural frequencies of the first two modes are very close between FE and EMA results. In these two modes, the large deformations appear to be on the CCOC and LPC. Compared to the first two modes, the deformations on the CCOC are significantly smaller in the other eight modes. Reducing the Young's modulus of HPC and LPC while increasing the Young's modulus of CCOC is possible to decrease the natural frequencies of the other modes while keeping the first two modes relatively unchanged.

For HPC and LPC, the Young's modulus of both parts should be decreased. Mode 5 and 6 have the largest NFD, where the large deformations concentrate on HPC, while both CCOC and LPC deforms moderately.

Based on these analyses, the Young's modulus of LPC should be decreased moderately while the Young's modulus of HPC should be decreased by a larger percentage. The Young's modulus of CCOC should be increased moderately, as the sole purpose of increasing Young's modulus for CCOC is to balance the natural frequency decrease in the first two modes because of the changes in HPC and LPC.

As described in the previous section, the initial Young's modulus is 100 GPa for all three parts. After several iterations, it is decided to increase the Young's modulus of CCOC by 30 GPa, decrease the Young's modulus by 30 GPa for LPC and 60 GPa for HPC. The results after the First Model Update (MU1) are shown in Table 3. It should be noted that, because of the excluded features and inaccurate geometries in the FE model, the Young's modulus of the materials in the FE model may not reflect the values of the materials used in the real structure, especially in the HPC where the thickness is very difficult to measure, and many small features are excluded during the creation of the FE model.

| Mode | 1 | 2 | 3 | 4 | 5 | 6 | 7 | 8 | 9 | 10 |
|---|---|---|---|---|---|---|---|---|---|---|
| Freq (Hz) | 39.198 | 39.391 | 49.332 | 49.334 | 57.755 | 57.818 | 82.572 | 82.577 | 129.59 | 129.59 |
| NFD (%) | 0.15 | -0.74 | -7.15 | -7.28 | -1.29 | -1.90 | 0.38 | 0.28 | 3.07 | 3.01 |

Table 3: Results of natural frequencies from FE analysis after MU1

The results verified that the overall strategy of the model update is correct, although mode 3 and 4 are overly adjusted. Following the same algorithm, the Young's modulus of LPC is increased, and to balance the first

two modes, the Young's modulus of CCOC is decreased. Eventually, the Young's modulus of HPC is adjusted slightly to fine-tune the natural frequencies.

The material properties after the model updates and the results from the FE modal analysis after the final model update are displayed in Table 4 and Table 5 respectively.

| | CCOC (Initial) | HPC (Initial) | LPC (Initial) | CCOC (MU1) | HPC (MU1) | LPC (MU1) | CCOC (Final) | HPC (Final) | LPC (Final) |
|---|---|---|---|---|---|---|---|---|---|
| Young's modulus (GPa) | 100 | 100 | 100 | 130 | 40 | 70 | 125 | 42 | 80 |

Table 4: Changes in material properties during the model updates

| Mode | 1 | 2 | 3 | 4 | 5 | 6 | 7 | 8 | 9 | 10 |
|---|---|---|---|---|---|---|---|---|---|---|
| Freq (Hz) | 39.379 | 39.569 | 52.808 | 52.811 | 58.674 | 58.737 | 89.684 | 89.689 | 141.03 | 141.03 |
| NFD (%) | 0.61 | -0.29 | -0.60 | -0.75 | 0.28 | -0.34 | 9.03 | 8.91 | 12.17 | 12.11 |

Table 5: Results of natural frequencies from FE analysis after the final model update

As the modal updating theory suggests, although the NFD values for the first six modes are very small, as the mode number increases, the discrepancies between the FE modal analysis results and EMA results increase correspondingly. Considering that the FE model is created manually based on the measured dimensions, as well as the exclusion of small features, the FE model after the final model update is considered acceptable in terms of natural frequencies.

With the natural frequencies of the FE model updated successfully, it is now necessary to compare the FE results and EMA results quantitatively in terms of the mode shapes. The quantitative method used to compare the mode shapes is Modal Assurance Criterion (MAC), which is defined as shown in Equation 2, where $\{\varphi_{FE}\}_i$ is the $i^{th}$ mode shape of the FE model and $\{\varphi_{EMA}\}_j$ is the $j^{th}$ mode shape from the EMA.

$$\mathrm{MAC}(i,j) = \frac{\left|\{\varphi_{FE}\}_i^T \{\varphi_{EMA}\}_j^*\right|^2}{\left(\{\varphi_{FE}\}_i^T \{\varphi_{FE}\}_i^*\right)\left(\{\varphi_{EMA}\}_j^T \{\varphi_{EMA}\}_j^*\right)} \tag{2}$$

A MAC value equal to one indicates a perfect correlation, and a MAC value equal to zero indicates zero correlation between these two mode shapes [5]. Generally, 80% is used as the threshold for good correlation between the two mode shapes. However, there is not a formal standard as MAC values vary from case to case. Simpler models tend to have higher MAC values while achieving an equivalently high MAC value for a complex model is significantly more difficult.

All mode shapes from the EMA and the FE modal analysis after the final model update are used to calculate the MAC. Necessary rotations of mode shapes were performed due to the symmetry of the structure. The calculated MAC plot is shown in Figure 4. The matched mode pairs and their MAC values are listed in Table 6, where mode pairs are in this format: EMA mode – paired FEA mode.

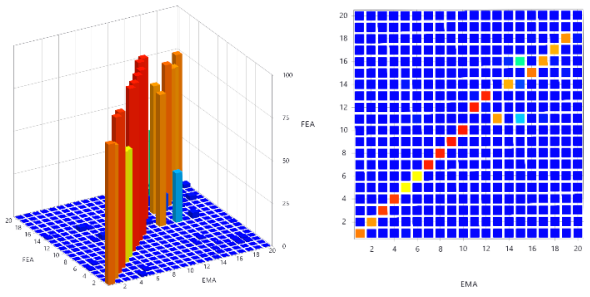


(a) (b)

Figure 4: MAC plot, FEA modes vs EMA modes

| Mode Pair | 1-1 | 2-2 | 3-3 | 4-4 | 5-5 | 6-6 | 7-7 | 8-8 | 9-9 | 10-10 |
|---|---|---|---|---|---|---|---|---|---|---|
| MAC (%) | 82.1 | 78.2 | 91.5 | 91.3 | 64.9 | 62.9 | 95.5 | 95.5 | 96.7 | 96.7 |
| Mode Pair | 11-13 | 12-12 | 13-12 | 14-14 | 15-16 | 16-15 | 17-16 | 18-17 | 19-18 | 20 |
| MAC (%) | 77.0 | 96.1 | 95.3 | 74.8 | 42.5 | 82.7 | 77.1 | 74.7 | 79.1 | |

Table 6: MAC values, EMA modes vs FEA modes

By inspecting the MAC values, it can be observed that in the first ten EMA modes, seven modes have found their correlated FE modes with MAC values greater than 80%. In the first 20 modes, there are ten mode pairs with MAC values greater than 80%, with another six MAC values close to 80%. By observing the mode shapes shown in Figure 3, modes with large deformations on LPC have higher MAC values while modes with large deformations on HPC have lower MAC values.

In summary, the FE model is acceptable in terms of both natural frequency and mode shape. The natural frequencies for the first 6 modes are very close between the EMA and FE results. As for mode shape, seven out of the first ten non-rigid FE modes have found their correlated EMA mode with MAC value greater than 80%. The LPC region has the highest correlation while the HPC region contributes poorly to the MAC values. The most likely reason is that there are many small features on the HPC of the aero-engine casing assembly that are excluded in the FE model, as shown in Figure 1. The accurate thickness of the HPC region is very difficult to measure, which is another possible factor that leads to the discrepancies. As a comparison, the LPC region has few small features so that a high agreement between the FE and EMA results is easily achieved.

Additionally, techniques such as Coordinate Modal Assurance Criterion (COMAC) can be used to identify the more precise locations of the nodes contributing poorly to the MAC values, so the inaccurately modelled regions can be located [6]. Because of the algorithm of COMAC, which is shown in Equation 3, it has high precision so that every individual node can be sorted according to its contribution to the MAC values. The geometries and material properties of these locations can be further updated to improve the correlations between the FEA and the EMA results.

$$\mathrm{COMAC}(k) = \frac{\left(\sum_{i=1}^{n} |(\varphi_A)_{ik}(\varphi_X)_{ik}^{*}|\right)^2}{\sum_{i=1}^{n}(\varphi_A)_{ik}^2 \sum_{i=1}^{n}(\varphi_X)_{ik}^{*2}} \tag{3}$$

In Equation 3, $(\varphi_A)_{ik}$ is the value, such as displacement, of the $k^{th}$ element in the $i^{th}$ analytical mode shape, $(\varphi_X)_{ik}$ is that value for the $i^{th}$ experimental mode and $n$ is the total number of correlated mode pairs. The COMAC, which is a vector, has the same size as the original mode shape vector and every node can be placed back to their original location, so the locations of the regions that contribute poorly to the MAC values can be revealed clearly. Although COMAC is not necessary here for model updating of this FE model, it is used and interpreted in this research, which is demonstrated in the next section of this paper.

## 4 Effects of changes in contact condition on dynamic behaviours

After the completion of the model update, several subsequent models are created, where different profiles are created for the interfaces. Figure 5 demonstrates the creation of the interfaces with different profiles, where a 2 mm deep annular gap is created on the top and bottom surfaces of HPC respectively. The location of the gap is selected so that the engineering fasteners pass through the gaps, by which the gaps can have considerable impacts on the behaviours of the fasteners. In total, 19 subsequent FE models are created, where the widths of the gaps are from 1 to 19 mm. The same FE modal analysis procedure is performed on every model. The changes in natural frequencies of the first six modes as the width of the gap increases are shown in Figure 6 (a) to (f) respectively, where OM represents 'Original intact model after the final model update' and CMx represents 'Created model with $x$ mm wide gap'.

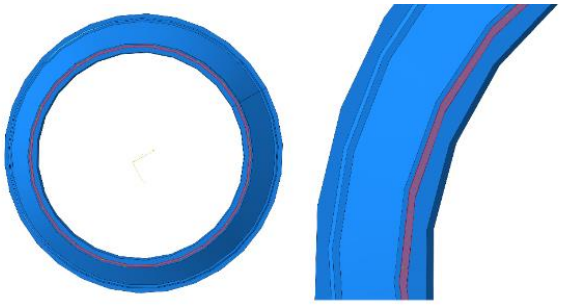

Figure 5: Creation of the alternate contact interface profile

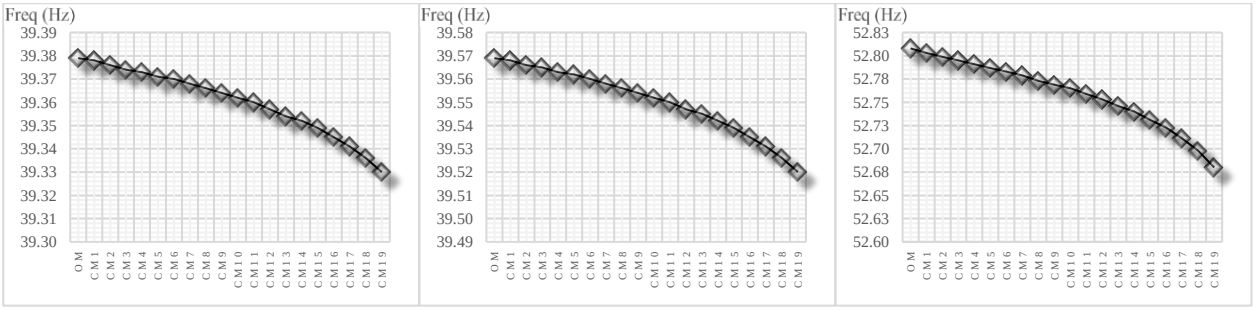


Figure 6: Changes in natural frequencies of the first six modes as the width of the gap increases

As demonstrated clearly in Figure 6, for every mode the natural frequency decreases monotonically as the width of the gap increases. Additionally, as the size of the gap increases, the changes in natural frequencies appear to be more drastic. The percentage changes in natural frequencies between OM and CM19 are listed in Table 7.

| Mode | 1 | 2 | 3 | 4 | 5 | 6 | 7 | 8 | 9 | 10 |
|---|---|---|---|---|---|---|---|---|---|---|
| OM (Hz) | 39.379 | 39.569 | 52.808 | 52.811 | 58.674 | 58.737 | 89.684 | 89.689 | 141.03 | 141.03 |
| CM19 (Hz) | 39.330 | 39.520 | 52.680 | 52.684 | 58.420 | 58.482 | 89.574 | 89.579 | 140.95 | 140.96 |
| NFD (%) | -0.124 | -0.124 | -0.242 | -0.240 | -0.433 | -0.434 | -0.123 | -0.123 | -0.057 | -0.050 |

Table 7: Percentage changes in natural frequencies between OM and CM19

This result seems counter-intuitive considering that the total mass of the model decreases as the width of the gap increases, which theoretically should increase the natural frequencies of the structure. A possible explanation is that the reduction of contact area changed both the mass and stiffness matrix of the model. Although the decrease in mass suggests increased natural frequency, the overall decreasing trend of natural frequencies as the width of the gap increases indicates that the stiffness of the structure has decreased. It is theoretically comprehensible that the overall stiffness of the structure decreases because the gaps created on

the interfaces make the model more flexible, which decreases the local stiffness. However, this explanation needs to be verified on this model.

Mathematically, strain energy can be used to reveal the changes in flexibility. The strain energy density for a volume element subjected to arbitrary stress can be calculated as described in Equation 4.

$$u = \frac{1}{2}\left(\sigma_{xx}\varepsilon_{xx} + \sigma_{yy}\varepsilon_{yy} + \sigma_{zz}\varepsilon_{zz}\right) + \left(\sigma_{xy}\varepsilon_{xy} + \sigma_{yz}\varepsilon_{yz} + \sigma_{zx}\varepsilon_{zx}\right) \tag{4}$$

$$= \frac{1}{2E}\left(\sigma_{xx}^2 + \sigma_{yy}^2 + \sigma_{zz}^2\right) - \frac{\nu}{E}\left(\sigma_{xx}\sigma_{yy} + \sigma_{yy}\sigma_{zz} + \sigma_{zz}\sigma_{xx}\right) + \frac{1}{2\mu}\left(\sigma_{xy}^2 + \sigma_{yz}^2 + \sigma_{zx}^2\right)$$

If the model has a higher strain energy after the gap is created, it suggests an increase in flexibility hence the decrease in stiffness. Strain energy density data for the first ten non-rigid modes of all 20 models are extracted. The strain energy density map of the 6th mode from the intact model OM, which is superimposed on its mode shape, is displayed in Figure 7 as an example to show the strain energy density distribution.

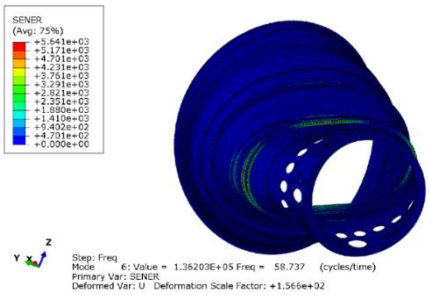


Figure 7: Strain energy density of the 6th mode from the original model

As for the data extraction, strain energy density at the integration points are selected, instead of the values at the individual nodes (element corners). In FE analysis, the integration points provide data with the highest accuracy, while the nodal solutions are extrapolated from the results at the integration points.

With the strain energy density data for every integration point extracted, the average strain energy density of the whole model can be calculated. The changes in average strain energy density of the first six modes as the width of the gap increases are shown in Figure 8 (a) to (f) respectively.

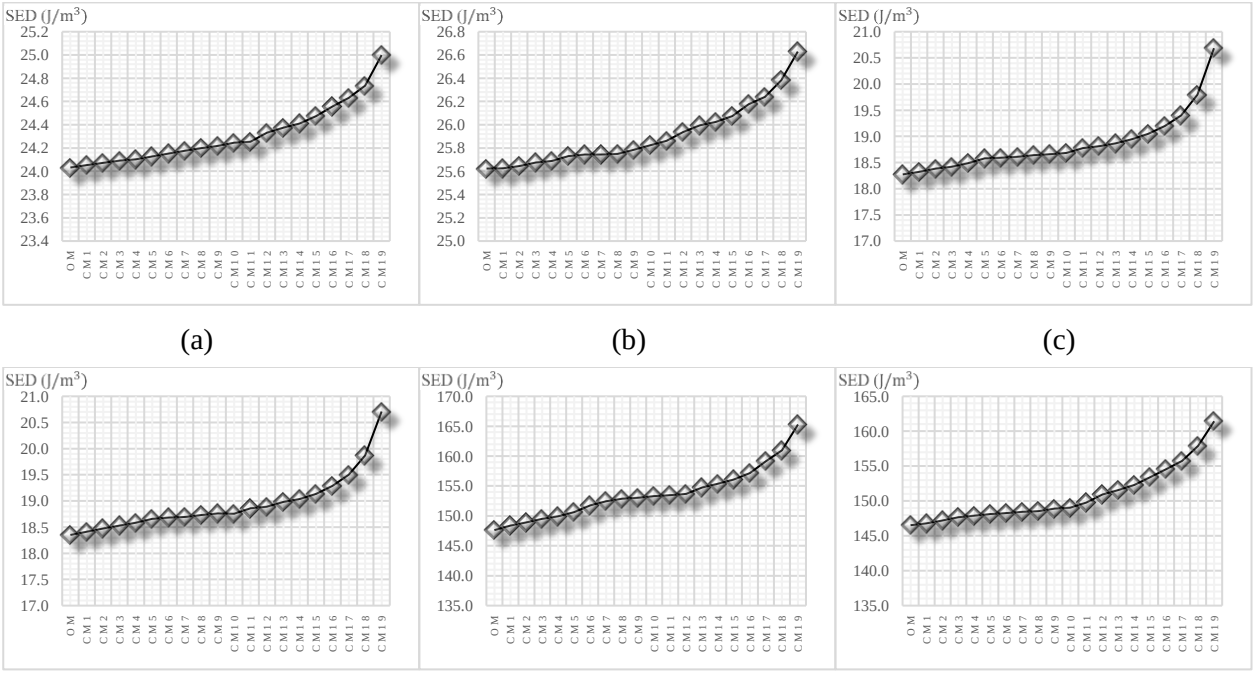


Figure 8: Changes in average strain energy density as the width of the gap increases

The average strain energy density of the structure increases monotonically with the size of the gap. The monotonic increase of average strain energy density confirms that the structure becomes more flexible as the size of the gap increases, which indicates the decrease in stiffness of the structure. Additionally, as the size of the gap increases, the decrease in stiffness becomes more drastic. Mathematically, the strain energy density in the interface regions is expected to approach infinity as the area of contact approaches zero because of the extremely high stress caused by the infinitesimal contact area, which can be derived based on Equation 4. This explains the reason why the natural frequencies change more drastically as the size of the gap increases.

By using strain energy, the decreases in the natural frequency of the structure have been explained. However, as demonstrated in Table 7, the natural frequencies changed differentially for the ten modes. It can be observed that the changes in mode 5 and 6 are significantly larger than the changes in other modes.

This phenomenon can be explained using strain energy as well. As the changes in geometry are made at the interface regions of the structure, the average strain energy density of the interface regions can be calculated for each mode and compared with the average strain energy density of the whole structure, based on which the relative impacts from the local changes in the interface regions on the overall dynamic behaviours of the structure can be evaluated.

To perform this task, the strain energy density data for both interfaces of the OM model are extracted, which include the strain energy density of integration points on all four surfaces constituting the two interface regions. The average strain energy density data of the interface regions are calculated and listed in Table 8, which also has the average strain energy density of the whole model and the ratio between them.

| Mode | 1 | 2 | 3 | 4 | 5 | 6 | 7 | 8 | 9 | 10 |
|---|---|---|---|---|---|---|---|---|---|---|
| $u_{int.}$ (J/m$^3$) | 17.50 | 18.58 | 22.94 | 22.99 | 291.81 | 293.16 | 25.14 | 21.66 | 18.45 | 18.54 |
| $u_{model}$ (J/m$^3$) | 24.03 | 25.62 | 18.27 | 18.35 | 147.63 | 146.53 | 35.86 | 31.19 | 59.29 | 59.38 |
| Ratio | 0.7680 | 0.7251 | 1.2554 | 1.2527 | 1.9767 | 2.0007 | 0.7011 | 0.6943 | 0.3113 | 0.3122 |

Table 8: Average strain energy density data of model OM

As displayed in Table 8, in mode 5 and 6 the average strain energy density in the interface regions are significantly higher than the average strain energy density of the whole model. The ranking of the ratio between strain energy densities matches exactly the ranking of the natural frequency change. In mode 5 and 6, the local changes in the interface regions have the highest impacts to the stiffness of the structure, which causes that the natural frequency changes in these two modes are significantly higher than the changes in the other modes. Similarly, in mode 9 and 10, the influences caused by the local changes in the interface regions are relatively small, which leads to smaller changes in natural frequencies.

To confirm that the changes in average strain energy density are caused by the gaps created on the interfaces, instead of other unexpected factors acting on other locations of the model, COMAC is used to compare the strain energy density data of CM1 and CM19. The strain energy density data for the first 10 non-rigid modes of both models are used. The calculated COMAC values of all nodes constituting the FE model and the recovered model with superimposed COMAC values are shown in Figure 9 (a) and (b).

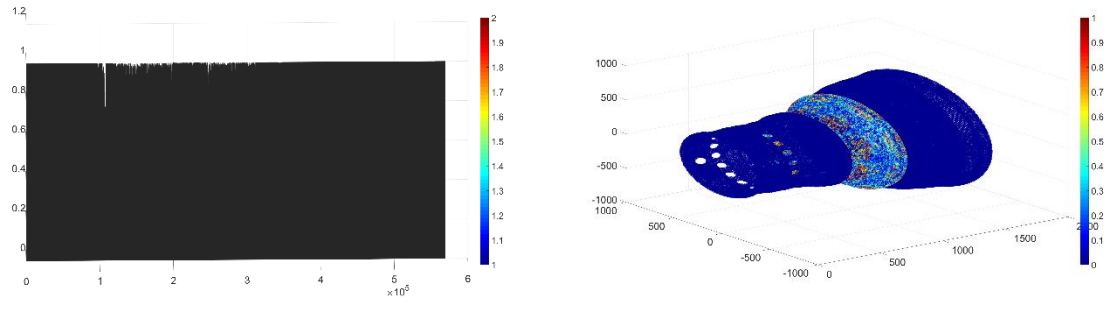

(a) (b)

Figure 9: COMAC between the first 10 non-rigid modes of CM1 and CM19

In Figure 9 (a), it is shown that for most of the nodes, their strain energy density values did not change or changed very slightly between CM1 and CM19. There are two regions in Figure 9 (a) that have noticeable decreases in COMAC, which indicates the strain energy density changed significantly in these regions. In order to determine the locations of these regions, the COMAC values are then superimposed onto the geometric grid of the engine model, which is created by exporting the coordinates of the nodes from Abaqus and importing them into MATLAB. The created figure is shown in Figure 9 (b). As a matter of fact, it is '$1 - \mathrm{COMAC}$' that is used in Figure 9 (b), so that nodes with smaller COMAC values will be in red hence more noticeable. In Figure 9 (b), it can be observed clearly that, these two regions with noticeably smaller COMAC values are the areas around these two interfaces. Nodes on HPC experience overall greater changes in terms of strain energy density compared to nodes on CCOC and LPC, which is comprehensible because they are influenced by both interfaces, while for nodes on CCOC or LPC the influence from one interface is always very small, even almost negligible.

By using COMAC, the locations with the most significant changes in strain energy density have been identified. It has been verified that the changes in natural frequencies are caused by the effects of creating gaps on the interfaces locally, which leads to a reduction in stiffness of the structure.

From this section of the research, it can be observed that, despite the decrease in mass of the structure caused by the creation of the gap on the interfaces, the natural frequencies of the structure still decrease because of the increased flexibility. The decrease in stiffness has been verified by the use of strain energy density. The extent to which the natural frequencies change can be evaluated based on the ratio between the average strain energy density of the interface regions and the average strain energy density of the whole model. It has also been shown that, apart from mode shapes, the COMAC is also capable of being used on other parameters, such as strain energy density in this case, to determine and locate the discrepancies between two sets of data.

## 5 Effects of changes in contact condition on thermal behaviours

In the second part of this research, the effects of changes in contact conditions on the thermal behaviours caused by the friction on the interfaces are studied. This is achieved by focusing on the energy loss due to friction using thermal parameters including temperature increase and frictional heat generation.

An important reason for studying the friction through energy loss is that contact friction is one of the main causes of nonlinear behaviours in coupled structures. If contact friction can be decreased, the nonlinear behaviours in the structure can be reduced effectively.

Theoretically, friction causes energy loss, during which heat is generated. The total frictional heat generation on area $A$ over time $t$ can be calculated as shown in Equation 5, where $P_{fr}$ is frictional heat generation of a unit area over time $t$, $\tau$ is shear stress and $\gamma$ is total length of the overall slip path, which is the total distance of the relative movement between the two surfaces [7].

$$P_A = \iint P_{fr}\, dA = \iint \tau\gamma\, dA \tag{5}$$

Shear stress in contact regions can be calculated from the contact pressure $p$ and friction coefficient $\mu$:

$$\tau = \mu p \tag{6}$$

Theoretically, the creation of gap on the interfaces will increase contact pressure, which increases shear stress hence accelerates frictional heat generation in a unit area on the contact region. However, the reduction in contact area is likely to decrease the total frictional heat generation. Additionally, the increased contact pressure is also possible to cause slip rate and slip distance to decrease.

All three factors determining the total frictional heat generation are affected by the changes in contact area. The contact pressure will increase, which causes an increase in shear stress but decrease in slip rate. The total contact area will also decrease. The combined effects of changes in the three factors make the total frictional heat generation very difficult to predict theoretically.

Because of the challenges in predicting the frictional heat generation theoretically and performing the test experimentally, accurate FE simulations must be performed to identify the effects caused by the changed contact conditions on the frictional heat generation and temperature increase in this structure.

In order to obtain accurate thermal results from FE analysis, a coupled temperature-displacement dynamic analysis must be used because of the mutual influences between the thermal and dynamic behaviours.

In general, the coupled temperature-displacement analysis requires extreme computational cost and time, which is one of the reasons that alternative methods have been used extensively for this type of analyses. Exporting the results from a dynamic analysis and importing them back to a thermal analysis is one of these theoretically sensible methods. This method requires considerably lower computational cost and time. However, the interactions between the thermal and dynamic behaviours are neglected in this method. These interactions can only be reflected in a fully coupled temperature-displacement analysis.

The FE model used in the first part of this research is too complicated for a coupled temperature-displacement analysis. Performing a coupled temperature-displacement analysis on it will be practically impossible even with a supercomputer. A new FE model is created, in which the model is further decreased to a more basic shape. The meshed model is shown in Figure 10. The element size for the interface regions is 20 mm with 10% minimum element size control. The rest of the model is meshed with 100 mm tetrahedral elements with 10% minimum element size control. The model is updated following a similar strategy used in the first part of this research.

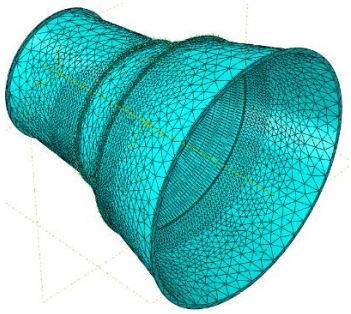

Figure 10: Meshed FE model for coupled temperature-displacement analysis

The input force has a frequency matching the natural frequency of the 5$^{th}$ and 6$^{th}$ mode of the structure to achieve resonance. The selection of this frequency for excitation is because it has been concluded that the interface regions have the highest impacts on the overall behaviours of the structure in these two modes. For the same reason, the location of the input force is selected to be located approximately at the middle of the outer surface of the HPC section, so that both interface regions can be excited effectively. The exact location is determined based on an algorithm for automatic selection of candidate sensor locations [8].

Due to the high computational cost and time of this analysis, the time period of the analysis cannot be extended to match a realistic test. As a compensation, a very high force magnitude is selected to scale the simulation so that there is a detectable amount of heat generation within the short time period of the simulation, which is only one second. It should be noted that plastic behaviours are excluded in this FE model, which means the model will not experience plastic deformation or damage under large forces, so the high force magnitude only acts for scaling purposes without being able to cause unexpected behaviours.

Additional material properties including thermal conductivity and specific heat capacity have been added, so that heat transfer can be simulated correctly. The boundary condition of this analysis is set to be free-free so only phenomena caused by the vibration of the structure itself are considered. The initial temperature of the structure is set to 20 degrees Celsius, so as the environmental temperature. Average temperature and frictional heat generation of the model are calculated at the end of the analyses, which are listed in Table 9.

It needs to be noted that, despite the decrease in complexity of the model and the use of a supercomputer, performing a coupled temperature-displacement analysis is still time-consuming. In this research, the coupled temperature-displacement analyses are performed on BlueCrystal, a High-Performance Computing (HPC) machine of University of Bristol. 64 Intel Xeon E5-2670 processors and 256GB of Random Access

Memory (RAM) are requested for each analysis, with which each analysis takes approximately 100 hours to complete.

| Temp. (℃) | Average | Increase | Percentage | Heat Gen. ($W/m^2$) | Average |
|---|---|---|---|---|---|
| OM | 20.00907 | 0.00907 | 0.045349% | OM | $2.57788 \times 10^2$ |
| CM3 | 20.21050 | 0.21050 | 1.052498% | CM3 | $1.25427 \times 10^4$ |
| CM6 | 20.19675 | 0.19675 | 0.983756% | CM6 | $8.29843 \times 10^3$ |
| CM9 | 20.12195 | 0.12195 | 0.609764% | CM9 | $4.12921 \times 10^3$ |
| CM12 | 20.06030 | 0.06030 | 0.301520% | CM12 | $2.13393 \times 10^3$ |
| CM15 | 20.03463 | 0.03463 | 0.173170% | CM15 | $1.21155 \times 10^3$ |
| CM18 | 20.02543 | 0.02543 | 0.127148% | CM18 | $9.47077 \times 10^2$ |

Table 9: Thermal data at the end of the coupled temperature-displacement dynamic analyses

It can be observed from the results that, after the gap is created, the frictional heat generation decreases as the size of the gap increases, which is likely caused by the decreased slip rate and reduced total contact area. However, due to the location of the gap, the creation of the gap will affect the effectiveness of the fasteners significantly, which is expected to have high impacts on the relative movement between the contact surfaces. The increased slip rate caused by this will benefit the frictional heat generation and temperature increase, which explains the significant discrepancies between the model OM and the models with the gap created.

It is comprehensible that the contact pressure will increase due to the reduced contact area, however, the changes in the slip rate and distance still need to be verified. In order to achieve this, the average total slip distance of the nodes (the total distance of the relative movements between the nodes in the two surfaces) on the interfaces are calculated and listed in Table 10.

| Slip dis. (m) | Int. 1 | Int. 2 | Average | Slip dis. (m) | Int. 1 | Int. 2 | Average |
|---|---|---|---|---|---|---|---|
| OM | 0.00026 | 0.00001 | 0.00013 | CM12 | 0.00122 | 0.00049 | 0.00085 |
| CM3 | 0.00310 | 0.00051 | 0.00181 | CM15 | 0.00117 | 0.00040 | 0.00079 |
| CM6 | 0.00233 | 0.00069 | 0.00151 | CM18 | 0.00091 | 0.00037 | 0.00064 |
| CM9 | 0.00145 | 0.00056 | 0.00100 | | | | |

Table 10: Average total length of the slip path of the nodes on the interfaces

It is demonstrated clearly that, as the width of the gap increases, the average slip distance of nodes on the interfaces decreases monotonically, which verifies the assumptions made at the beginning of this section. Similar to the phenomena observed in the thermal data, the creation of gap alters the relative motion between the contact surfaces significantly, which causes distinct differences between models with and without the gaps on the interfaces.

In summary, as the width of the gap increases, the contact pressure will increase but the slip rate and total contact area will decrease. Despite the fact that the increased contact pressure may accelerate frictional heat generation in each unit area on the contact region, the reductions in contact area, slip rate and slip distance are able to cause more significant influences that surpass the influences from increased contact pressure so a monotonic relationship between the frictional heat generation and size of the gap is obtained. The combined effects of the three parameters cause total frictional heat generation to decrease as the size of the gap increases. However, the creation of the gap will affect the effectiveness of the fasteners, which increases the temperature rise and total frictional heat generation significantly.

For the sake of completeness, running a coupled temperature-displacement dynamic analysis on a complex FE model is achievable by using mass scaling to alter the time increment so that the total number of iterations

can be controlled. However, mass scaling can only be used situationally as using mass scaling can put the accuracy of the results in risk [9], which is one of the main reasons that it is not used in this research.

# 6 Discussions and conclusions

In this research, the effects of changing contact conditions of interface regions in an aero-engine casing assembly on its dynamic and thermal behaviours have been studied by using FE methods.

Firstly, the creation of the FE model and the mesh configurations have been explained. The model updating strategy for a manual model update of a complex coupled structure, such as the aero-engine casing assembly in this research, has been demonstrated. It has been shown that, without the usage of model updating software, performing model updates on a complex coupled structure is still possible to succeed. It has also been demonstrated that MAC and NFD can be used as the two main criteria for a model update to guide the model updating process to success. Additionally, the COMAC is available for more precise model improvements if model updates based merely on MAC and NFD are unable to obtain a decent FE model.

In the frequency domain analysis section of this research, it has been confirmed that local changes on the interfaces in a coupled structure are able to alter its dynamic responses and modal parameters. This research shows that, despite the decrease in total mass of the structure due to the creation of the gap on the interfaces, the natural frequency is still possible to decrease because of the increased flexibility and decreased stiffness in the structure. Additionally, it has been demonstrated that the sensitivity to same changes in contact conditions can be different for each mode. Some modes appear to be more sensitive than the others, which has been explained by calculating the ratio of average strain energy density in the interface regions to the average strain energy density of the whole model. The results showed high agreements between the trends of changes in strain energy density and changes in natural frequency, which concludes that strain energy density is capable of predicting and explaining the changes in dynamic responses and modal parameters of the structure by revealing the changes in stiffness. Additionally, it has been shown that the COMAC is capable of being used on parameters apart from mode shapes, such as strain energy density in this research, where it demonstrates successfully that it is the creation of gaps locally on the interfaces that affected the dynamic behaviour of the entire structure.

In the time domain part of this research, frictional heat generation and temperature increase are used to demonstrate that, besides dynamic behaviours, local changes on interfaces are also able to alter the thermal behaviours of the structure. The mathematical relationship between the temperature increase (or total frictional heat generation) and size of the gap is apparently monotonic, despite the opposite influences from the three determining parameters. The creation of the gap, however, alters the effectiveness of the fasteners significantly because of its location, which amplified the frictional heat generation greatly.

It has been shown that alternate designs for the interfaces are able to change the friction in the contact areas, which may benefit the control of nonlinear behaviours. Although the alternate profile of contact regions in this research caused an increase in friction because of the location of the gap, it shows the possibility of controlling the friction in the interface regions using an alternate contact profile, with which the nonlinear behaviours in the structure can be reduced effectively.

Despite the successes of obtaining and analysing the results and observations in this research, there are several potential improvements that can be made.

Firstly, it is possible to increase the quality of the FE model further by using COMAC to locate the small regions on the FE model that have large disagreements with the EMA structure.

In the frequency domain analysis, despite the changes in the width of the gaps, its depth was kept constant at 2 mm in this research. It is worth studying if a deeper gap is able to cause different results. As a matter of fact, the change in mass caused by a 2 mm deep gap is very small. It is possible that with a deeper gap or a change in profile, the effects from reduced mass may surpass the effects caused by the reduced stiffness, which eventually lead to an overall increase in natural frequency. Moreover, the changes in natural frequencies are not very large in this research, performing a similar study on a coupled structure with more and larger interface regions can be valuable. For this specific research on the aero-engine casing assembly,

it is also possible to continue increasing the width of the gap, to verify if the changes in strain energy density and local stiffness of the interface regions and changes in the natural frequencies of the structure are still able to become more drastic as the size of the gap increases.

In the time domain analysis, it has been mentioned that a simplified FE model was used due to the limitations of computational time and cost. It is possible to use an FE model with a higher quality mesh, like the model used in the frequency domain analysis of this research, to repeat this time domain analysis and study if the results can be different. In this research, the structure was stimulated by a single-point sinusoidal force that matches the natural frequency of the $5^{th}$ and $6^{th}$ mode. Changing the excitation frequency so that it matches the natural frequency of the first 10 or 20 non-rigid modes respectively to study if the differences in sensitivity between modes that appeared in the frequency domain analysis are still significant in the time domain analysis is also a potential direction for the future work of this research. Additionally, it might be necessary to study the changes in parameters when several random loads are applied at several different locations on the structure simultaneously, which is closer to the actual working condition of the structure so that the results can have higher values for practical applications. For this specific research, the size of the gap can be further increased to evaluate if the monotonic relationship between total frictional heat generation and size of the gap still holds when the size of the gap keeps increasing.

Finally, it might be worth trying to repeat the analyses performed in this research experimentally, although a simpler coupled structure could be used as an alternative because of the high cost for producing several samples of this complex aero-engine casing assembly.

## References

[1] D. Di Maio, Z. Mitha, J. V. Paul and X. Chi, "Variability of Dynamic Response in Jointed Structures," in *Dynamics of Coupled Structures, Volume 4. Proceedings of the 35th IMAC, A Conference and Exposition on Structural Dynamics 2017*, Garden Grove, CA, USA, 2017.

[2] R. L. Norton, Design of Machinery, New York City: McGraw-Hill Education, 2008.

[3] "37.1.2 Contact pressure-overclosure relationships," in *Abaqus Analysis User's Guide*, Dassault Systèmes Simulia Corp., 2016.

[4] "6.3.5 Natural frequency extraction," in *Abaqus Analysis User's Guide*, Dassault Systèmes Simulia Corp., 2016.

[5] R. J. Allemang, "The Modal Assurance Criterion (MAC): Twenty Years of Use and Abuse," University of Cincinnati, Cincinnati, OH, USA, 2003.

[6] N. A. J. Lieven and D. J. Ewins, "Spatial Correlation of Mode Shapes, The Coordinate Modal Assurance Criterion (COMAC)," in *Proceedings of the Sixth International Modal Analysis Conference*, Orlando, FL, USA, 1988.

[7] H. Schmidt, J. Hattel and J. Wert, "An analytical model for the heat generation in friction stir welding," *Modelling and Simulation in Materials Science and Engineering*, vol. 12, p. 143–157, 2004.

[8] FEMtools Pretest and Correlation Analysis User's Guide, Dynamic Design Solutions, 2016.

[9] "11.6.1 Mass scaling," in *Abaqus Analysis User's Guide*, Dassault Systèmes Simulia Corp., 2016.